Published in final edited form as:
Biochem Biophys Res Commun. 2010 November 19; 402(3): 537–542. doi:10.1016/j.bbrc.2010.10.071.

Myosin Light Chain Mono- and Di-Phosphorylation Differentially Regulate Adhesion and Polarity in Migrating Cells

Miguel Vicente-Manzanares[1] and **Alan Rick Horwitz**
Department of Cell Biology, University of Virginia School of Medicine; Charlottesville, VA 22908

Abstract

Myosin II is a critical regulator of cell migration that generates polarity, controls protrusion, and promotes adhesion maturation and retraction of the rear. Myosin II has an ATPase motor domain that is regulated by phosphorylation of the regulatory light chain (RLC) on Thr18 and Ser19. Here, we address the activation and specific function of the two phosphorylation states of the RLC, mono- (S19) and/or di-phosphorylation (T18+S19), in cell polarity and adhesion. Specific phospho-antibodies reveal that adhesion to fibronectin via the α5β1 integrin promotes localized mono- and di-phosphorylation of the RLC that follow different kinetics. Using phospho-mimetic mutants, we show that mono-phosphorylation promotes adhesion maturation in protrusions resulting in focal adhesions throughout the cell. In contrast, di-phosphorylation produces large, stable actomyosin bundles and large, non-dynamic adhesions that define the rear. Finally, RLC phosphorylation regulates the assembly and stability of MIIB, but not MIIA. Our data reveal a novel mechanism by which the degree of phosphorylation of the RLC differentially controls cell adhesion and polarity.

Keywords

Cell migration; polarity; adhesion; myosin II; phosphorylation

INTRODUCTION

Cell migration is essential for normal development, homeostasis, and regeneration. Also, a number of important diseases, like invasive cancer, autoimmune disease, and atherosclerosis, have a central, migratory component [1–3]. Cell migration is comprised of interdependent component processes that include front-back polarization, protrusion, adhesion, and rear retraction [4]. Adhesions are regions of contact with the substratum that serve two functions: they generate traction by connecting the extracellular matrix to the actin cytoskeleton, and they develop signals that regulate adhesion and actin polymerization, organization, and contraction [5].

[1]Correspondence: mvicente@virginia.edu.

Supplemental movies
Time-lapse of protrusions formed by cells co-expressing paxillin-mOrange and GFP-coupled *wild type* RLC (movie 1), -D,A (movie 2), -A,D (movie 3), or -D,D (movie 4)-GFP on fibronectin. Paxillin is shown in magenta, RLC mutants are in green. All movies were captured using TIRF microscopy (see M&M) at 1 frame/ 5s, and are played at 20 frames/s.

Myosin II has emerged as a major regulatory endpoint for cell migration, and plays a key role in each of the component processes. Myosin II is required for adhesion maturation, formation of large actin bundles, and retraction of the trailing edge [6,7]; it also serves to integrate forces in mechanotransduction. Myosin II is a bipolar actin motor comprised of two heavy chains (MHCII) and four light chains, two structural (essential, ELC) and two regulatory (RLC). There are three isoforms of the heavy chain, MHCII-A, -B and -C, which define three myosin II structural units, MIIA, MIIB and MIIC (reviewed in [8]). RLC displays multiple phosphorylation sites that regulate MII activity. Phosphorylation of Ser19 activates of the motor domain of the MHCII. Phosphorylation of Thr18 in the presence of phospho-Ser19 has an additive effect on the ATPase activity (K_{ATPase}) of the heavy chain [9]. There is also evidence that RLC phosphorylation controls myosin II assembly into filaments through conformational changes [10,11]. While both single (S19) and dual (T18+S19) phosphorylations are seen in migrating cells, their effect on the component processes of migration have not been addressed.

In this study, we parse the roles of RLC mono- and di-phosphorylation on adhesion and polarity in migrating cells. We find that adhesion to fibronectin promotes both mono- and di-phosphorylation; however, mono-phosphorylation occurs throughout the cell, whereas di-phosphorylation is restricted to the rear. Using a series of phospho-mimetic mutants, we find that mono-phosphorylation, particularly on Ser19, promotes adhesion maturation within protrusions, resulting in a relatively homogeneous population of focal adhesions throughout the cell. In contrast, di-phosphorylation induces large adhesions and actomyosin bundles, but only in a localized region of the cell, the rear. Our data also reveal a highly graded effect of these phosphorylations on the affinity/stability of MIIB, but not MIIA, in actomyosin filament bundles. These observations point to different roles for mono- and di-phosphorylated RLC in cell migration, and suggest that di-phospho-RLC-dependent stabilization of the myosin II assemblies plays an important role, in addition to the additive effect of mono- and di-phosphorylation of the RLC on the ATPase activity of the associated heavy chain [12].

MATERIALS & METHODS

Plasmids

GFP-MHCII-A and GFP-MHCII-B were gifts from Robert S. Adelstein [13]. RLC-GFP (*wild type* RLC) and RLC 18,19D-GFP (RLC-D,D-GFP) were kindly provided by Kathleen Kelly (National Cancer Institute, Bethesda, MD). The RLC T18, S19 mutant combinations (DA, AD) were generated by site-directed mutagenesis and verified by DNA sequencing. Where indicated, GFP was replaced with mCherry, a gift from Roger Tsien [14]. Paxillin-mOrange (CoralHue^{TM} monomeric Kusabira Orange, from MBL) has been described previously [15].

Antibodies and reagents

The following antibodies were used: MHCII-A and MHCII-B (rabbit, pAb) from Covance; phosphorylated RLC~P (S19) and RLC~P,P (T18+S19) (rabbit, pAb), from Cell Signaling; RLC (MY-21, mAb), β-tubulin (TUB2.1, mAb) and vinculin (hVin-1, mAb), from Sigma. Secondary anti-mouse and anti-rabbit antibodies conjugated to Alexa488, 568 and 647 were from Invitrogen; HRP-conjugated anti-mouse and anti-rabbit antibodies, from Pierce. Rhodamine-X-conjugated phalloidin was from Cytoskeleton Inc. Fibronectin was from Sigma.

Cell culture and transfection

CHO-K1 cells (ATCC) were cultured in low-glucose DMEM supplemented with 10% FBS, 4 mM L-glutamine, 1 mM sodium pyruvate, 1% (vol/vol) nonessential amino acids, and penicillin/streptomycin and transfected with 0.25–1 μg DNA using Lipofectamine (all from Invitrogen). For imaging assays, cells were plated on glass-bottomed dishes preincubated overnight with 2 μg/ml fibronectin, in CCM1 for 1 h and maintained at 37°C at pH 7.4 (migration promoting conditions).

Western blot

CHO.K1 cells plated as indicated in the figures, and extracted with 1% Nonidet P-40 (Fluka) in PBS containing 1 mM $MgCl_2$, 5 mM ATP, protease and phosphatase inhibitors (all from Sigma) and the extract was centrifuged at 14000xg for 15 min. The supernatant was subsequently mixed with Laemlii buffer, fractionated in 4–20% gradient PAGE/SDS (BioRad), transferred to PVDF membranes (BioRad), and blotted as indicated.

Immunofluorescence

Cells were allowed to adhere to fibronectin (FN)-coated coverslips (2 μg/ml) for 45 min, fixed using 4% methanol-free formaldehyde and permeabilized with 0.5% Triton X-100 for 10 min. The coverslips were blocked using 0.1% IgG-free BSA for 30 min, and incubated with primary antibodies and a species-appropriate secondary antibody coupled to either Alexa488 or Alexa647 as indicated. For actin staining, phalloidin conjugated to Rhodamine X was used.

Microscopy and image processing

Confocal images were collected on an Olympus Fluoview 1000 microscope (IX81 base) equipped with a 60x /1.35 NA (oil) UPLSAPO 60x objective (Olympus). Green probes (GFP and Alexa488) were excited using the 488 nm laser line of a multi Ar laser; red probes (mCherry, Alexa568 and Rhodamine X) were excited with the 543 nm laser line of a He-Ne laser; the far-red probe Alexa647 was excited with the 635 nm line of an LD laser. Fluorescence emission was collected using the following dichroic mirror/filter combinations: SDM560/BA505–525 (GFP and Alexa488), SDM640/BA560–620 (mCherry, Alexa568 and RhodamineX) and BA655–755 (Alexa647). Three-color fluorescence images of Alexa488 (GFP)/Alexa568 (RhodamineX/mCherry)/ Alexa647 were collected in sequential mode. Images were acquired using Fluoview software (Olympus).

TIRF images were acquired on an Olympus IX70 inverted microscope. The excitation laser lines used were 488 nm (Ar laser) for GFP and 543 nm (He/Ne) for mOrange/mCherry. A dichroic mirror (HQ485/30) was used for GFP-labeled cells. For dual GFP- mCherry/ mOrange, a dual emission filter (z488/543) was used. Images were acquired with a charge-coupled device camera (Retiga Exi; Qimaging) and analyzed using Metamorph.

Myosin assembly assay

CHO.K1 cells were transfected with the indicated RLC mutants, allowed to adhere to fibronectin, and then soluble and insoluble pools containing endogenous MHCII-A and -B were separated by sequential fractionation. The cells were initially extracted with 1% Nonidet P40 in PBS containing protease and phosphatase inhibitors (Sigma) and the extract was centrifuged at 10000xg for 15 min. The supernatant is the “soluble fraction”. The pellet was subsequently solubilized using RIPA/Laemlii buffer, fractionated by PAGE/SDS, blotted with antibodies against MHCII-A, -B, and β-tubulin (which appears in both fractions; its solubility is not affected by RLC expression), as a loading control.

Fluorescence recovery after photobleaching (FRAP)

Confocal images for FRAP analysis were acquired using an Olympus Fluoview 300 microscope using a 60x /1.45 NA (oil) PlanApo 60xOTIRFM objective (Olympus). GFP and mCherry-coupled probes were excited using the 488 nm laser line of an Ar ion laser and the 543 nm laser line of a He-Ne laser (Melles Griot), respectively. Fluorescence emission was collected using SDM560 and BA505–525 (EGFP) and BA560–660 (mCherry) filters. Initially, a cellular area (34.72 μm^2) that contained actomyosin bundles decorated with GFP-MHCII-A or II-B in the presence of the corresponding RLC-mCherry mutant was scanned 3 times; then, a small region covering exclusively a segment of the bundle was selected and bleached using 15 scans at 100 % laser power. To image the fluorescence recovery of fluorescence intensity following the photobleaching, we did 15 scans every 0.1 sec, 15 scans every 3 sec, 14 scans every 5 sec, and 2 scans every 10 sec using 0.5% laser power. We then subtracted the background and accounted for overall bleaching during acquisition using a non-bleached portion of the target bundle. Finally, normalized intensity vs. time (sec) were plotted and fitted by a single exponential equation (R^2>0.98).

Adhesion dynamics

CHO.K1 cells were transfected with the indicated RLC mutants coupled to GFP, paxillin-mOrange and adhered to 2 μg/ml fibronectin for 45 min. Cells were filmed using TIRF microscopy and sequential movies collected for 15 min (1 image every 5 s). The movies were analyzed using ImageJ. The % of adhesions that disappeared from protrusions was analyzed in individual cells by plotting the normalized intensity of the adhesion over time.

RESULTS

Integrin-mediated adhesion to fibronectin induces an asymmetric distribution of mono- and di-phosphorylated RLC

Adhesion to fibronectin activates myosin II [6]; but how it affects RLC mono- vs. di-phosphorylation is not known. To address this, we used phospho-specific antibodies that distinguish between phosphorylation on S19 (RLC~P) and T18+S19 (RLC~P,P) in CHO.K1 cells, which express the fibronectin receptor α5β1. Cells were either kept in suspension or plated on different concentrations of fibronectin for 45 min, a time at which migration is robust [15]. Adhesion to fibronectin increased, even at low fibronectin concentrations, both RLC~P and RLC~P,P, when compared to cells in suspension (Fig. 1A). RLC~P increased modestly with the concentration of fibronectin; whereas RLC~P,P was dose-independent. We also examined the kinetics of RLC phosphorylation in cells plated on migration-promoting concentrations of fibronectin (1 μg/ml, Fig. 1B). RLC~P increased with time; whereas RLC~P,P reached an early plateau and remained stable for the duration of the experiment.

We used then localized mono- and di-phosphorylated RLC in CHO.K1 cells using the antibodies used above. We observed a gradient of structures decorated with RLC~P. Within protrusions, RLC~P was in puncta, which often decorated the actin bundles juxtaposed to the distal part of elongating adhesions (Fig. 1C, dotted boxes) but was absent near the leading edge (Fig. 1C). RLC~P was also present in thick actin bundles that terminate in large adhesions along the sides of cells that showed a pronounced trailing edge (Fig. 1C). In contrast, RLC~P,P was seldom observed in protrusive areas (Fig. 1D, boxes). Instead, it localized preferentially in the perinuclear region and in thicker actomyosin bundles that define the sides and rear of the cell (Fig. 1D, arrows).

Taken together, these results show that both RLC~P and RLC~P,P are stimulated by adhesion to fibronectin via the α5β1 integrin. However, their different localization strongly points to different roles in migration.

Furthermore, their different kinetics and dose dependence suggest that RLC~P is not a general, rate-limiting precursor of RLC~P,P throughout the cell. Instead it is likely phosphorylated by a localized kinase.

RLC mono- and di-phosphorylation on S19 and T18+S19 induce different effects on adhesion maturation and cell polarity

Based on their specific localization, our working hypothesis is that RLC~P induces adhesion elongation and growth throughout the cells, whereas RLC~P,P mediates formation of stable, non-dynamic actomyosin filaments and adhesions. To test this, we made three mutants: a di-phosphomimetic RLC-T18D/S19D (RLC-D,D); and two mono-phosphomimetics, RLC-T18D/S19A (RLC-D,A) and RLC-T18A/S19D (RLC-A,D). Whereas Asp (D) is phospho-mimetic, Ala (A) is non-phosphorylable, ensuring that the mutant RLC cannot be phosphorylated on the adjacent site. Cells expressing RLC-A,D, but not RLC-D,A, exhibit large, numerous adhesions throughout the cell (Fig. 2A). In addition, both RLC-D,A and RLC-A,D mutants distribute throughout the entire cell, as does *wild type* RLC (Fig. 2A). In contrast, RLC-D,D generates very large adhesions adjacent to thick, RLC-D,D-decorated actomyosin bundles (Fig. 2A, arrowhead). Strikingly, these structures were confined to a single region of cell. Thus, the localization or mono- vs. di-phosphorylation appears to dictate the differential localization, adhesion maturation and polarity, rather than responding to it.

To determine the origin of these differences, we co-transfected CHO.K1 cells with each of the RLC mutants coupled to GFP and the adhesion marker paxillin coupled to mKusabira Orange (mOrange) and then imaged their dynamics using TIRF microscopy. RLC-A,D increased the fraction of nascent adhesions that undergo maturation, thereby producing in a general increase in focal adhesions throughout the cell (Fig. 2D,F and Supplemental movie 3). The adhesions in RLC-D,A expressing cells (Fig. 2C and Supplemental movie 2) matured similarly to those expressing *wild type* RLC (Fig.2B,F and Supplemental movie 1). In contrast RLC-D,D accumulated in a single region that established the rear as the cell moved away from it, and produced abnormally large and stable adhesions in its vicinity (Fig. 2A,E,F and Supplemental movie 4). However, adhesions in protruding regions (normally opposite the RLC-D,D-decorated rear) remained small and dynamic (Fig. 2F). These data show that RLC-S19~P mediates general adhesion maturation; whereas RLC~P,P localizes adhesion maturation to the region that defines the rear [16]. The striking and surprising phenotypic differences between the RLC-D and RLC-D,D mutants are not readily explained by its reported effects on ATPase activity per se. It suggests that another role for RLC phosphorylation might be involved, e.g., differential effects on myosin II filament assembly or stability, which have been observed biochemically for smooth muscle myosin but not for non-muscle myosin II in live cells.

RLC~P and RLC~P,P differentially modulate MIIB assembly and stability

To determine whether RLC~P,P and RLC~P differentially control myosin filament assembly and stability, we measured the stability of MIIA and MIIB filaments - the two spatially segregated isoforms present in CHO.K1 cells [7]. We expressed the mono- and di-phosphomimetic RLC mutants and assayed their solubility, which measures filament assembly and stability [17], of endogenous MIIA and MIIB at low salt. The RLC mutants show a graded effect on MIIB solubility. RLC-D,D produced the highest degree of insolubility; RLC-A,D also increased MIIB insolubility, although to a lower extent. RLC-

D,A had no significant effect when compared to *wild type* (Fig. 3A). In striking contrast, all these mutants had a small, if any, effect on the solubility of MIIA (Fig. 3A). These data show that MIIB forms stable bundles that are stabilized by phosphorylation of the RLC; whereas, MIIA assembly is largely independent of RLC phosphorylation.

We then confirmed and extended the solubility observations using FRAP, which measures the exchange rate between myosin IIA or IIB and actomyosin filaments and can be used to estimate the affinity [18]. We co-expressed the RLC mutants with MHCII-B or MHCII-A (which do not co-assemble in the same filaments but form stippled patterns [7,19]), and then measured the FRAP of the heavy chains (coupled to GFP) that underlies and is bound to the corresponding RLC mutant (visualized by a mCherry tag). With RLC-D,D, only a small fraction of the MIIB recovered (Fig. 3C), which is consistent with a previous report [16], and demonstrates its high effective affinity for the bundles. However, RLC-D,D had a negligible effect on MIIA (Fig. 3B and [16]). Interestingly, RLC-A,D had an intermediate effect on the affinity of MIIB and also had no effect on MIIA (Fig. 3B–C).

Together, these data show that the phosphorylation state of RLC differentially affects MIIB vs. MIIA binding to actomyosin filaments. They also reveal a differential effect of RLC phosphorylation on MIIB affinity for actomyosin filaments and suggest that the differential effect of RLC~P and RLC~P,P on adhesion and actomyosin localization resides, in part, on its effect on MIIB.

DISCUSSION

The data presented here suggests a model for how RLC regulates myosin II in cell migration. In this model, myosin II activation by either mono- or di-phosphorylation of the RLC (RLC~P) promotes adhesion maturation of its associated adhesions, which is suggested to regulate adhesive signaling to Rho GTPases [20–22]. However, di-phosphorylation (RLC~P,P) produces large, highly stable, localized bundles, and thereby induces maturation of the associated adhesions. This defines a region that becomes the rear as the leading edge moves away it. The differential kinetics of phosphorylation and segregation of RLC~P,P suggest the importance of a specific, localized kinase. One candidate is Rho-kinase (ROCK), which is reported to regulate rear retraction in migrating cells [23].

How does RLC phosphorylation regulate the different functions of myosin IIB in front-back polarity and adhesion maturation? *In vitro* kinetic and motility studies using RLC~P and ~P,P on the smooth muscle myosin II isoform show that RLC increases the ATPase activity, which arises from differences in K_{ATPase}, the apparent dissociation constant for the heavy chain from actin of the heavy chain for actin; however it had no effect on the V_{max} or the *in vitro* motility of actin filaments, which is an indicator of contractility. Therefore, increasingly phosphorylated RLC induces thicker actomyosin bundles and larger associated adhesions due to the increased affinity of phosphorylated RLC-bound myosin IIB to other myosins through the tail domain [16,24], and to actin filaments through the head domain, an effect that is not seen for myosin IIA. RLC phosphorylation is also proposed to regulate a conformational change that opens a head-tail association that inhibits myosin II filament assembly [10,11] and results in an assembly-competent state [25]. In this regard, a mutant of the heavy chain unable to bind RLC cannot revert back to the assembly-incompetent state [17]. Our data show that this occurs mainly through the differential effect of RLC phosphorylation (RLC~P,P > RLC~P) on MIIB stability in actomyosin bundles, and suggests that the biological effects of the phospho-mimetic mutants are based, at least in part, on the inhibition of the head-tail association of MIIB.

This explains why RLC-D,D fails to induce actomyosin bundling in MIIB-depleted cells, which contain only MIIA [16]. Remaining challenges include elucidating the kinases that regulate mono vs. di-phosphorylation, and the synergy betwenne myosin II-mediated polarity and other molecular mechanisms implicated in cell polarization, e.g. microtubules, and how myosin II affects signalling.

Supplementary Material

Refer to Web version on PubMed Central for supplementary material.

Acknowledgments

This work was supported by NIH grants GM23244 (AFH) and the Cell Migration Consortium (U54 GM064346). The authors also thank Leanna Whitmore for technical support.

References

1. Ridley AJ, Schwartz MA, Burridge K, Firtel RA, Ginsberg MH, Borisy G, Parsons JT, Horwitz AR. Cell migration: integrating signals from front to back. Science. 2003; 302:1704–1709. [PubMed: 14657486]
2. Friedl P, Wolf K. Plasticity of cell migration: a multiscale tuning model. J Cell Biol. 2010; 188:11–19. [PubMed: 19951899]
3. Olson MF, Sahai E. The actin cytoskeleton in cancer cell motility. Clin Exp Metastasis. 2009; 26:273–287. [PubMed: 18498004]
4. Vicente-Manzanares M, Webb DJ, Horwitz AR. Cell migration at a glance. J Cell Sci. 2005; 118:4917–4919. [PubMed: 16254237]
5. Vicente-Manzanares M, Choi CK, Horwitz AR. Integrins in cell migration--the actin connection. J Cell Sci. 2009; 122:199–206. [PubMed: 19118212]
6. Chrzanowska-Wodnicka M, Burridge K. Rho-stimulated contractility drives the formation of stress fibers and focal adhesions. J Cell Biol. 1996; 133:1403–1415. [PubMed: 8682874]
7. Vicente-Manzanares M, Zareno J, Whitmore L, Choi CK, Horwitz AF. Regulation of protrusion, adhesion dynamics, and polarity by myosins IIA and IIB in migrating cells. J Cell Biol. 2007; 176:573–580. [PubMed: 17312025]
8. Vicente-Manzanares M, Ma X, Adelstein RS, Horwitz AR. Non-muscle myosin II takes centre stage in cell adhesion and migration. Nat Rev Mol Cell Biol. 2009; 10:778–790. [PubMed: 19851336]
9. Umemoto S, Bengur AR, Sellers JR. Effect of multiple phosphorylations of smooth muscle and cytoplasmic myosins on movement in an in vitro motility assay. J Biol Chem. 1989; 264:1431–1436. [PubMed: 2521481]
10. Trybus KM, Lowey S. Conformational states of smooth muscle myosin. Effects of light chain phosphorylation and ionic strength. J Biol Chem. 1984; 259:8564–8571. [PubMed: 6610679]
11. Craig R, Smith R, Kendrick-Jones J. Light-chain phosphorylation controls the conformation of vertebrate non-muscle and smooth muscle myosin molecules. Nature. 1983; 302:436–439. [PubMed: 6687627]
12. Ikebe M, Hartshorne DJ. Phosphorylation of smooth muscle myosin at two distinct sites by myosin light chain kinase. J Biol Chem. 1985; 260:10027–10031. [PubMed: 3839510]
13. Wei Q, Adelstein RS. Conditional expression of a truncated fragment of nonmuscle myosin II-A alters cell shape but not cytokinesis in HeLa cells. Mol Biol Cell. 2000; 11:3617–3627. [PubMed: 11029059]
14. Shaner NC, Campbell RE, Steinbach PA, Giepmans BN, Palmer AE, Tsien RY. Improved monomeric red, orange and yellow fluorescent proteins derived from Discosoma sp. red fluorescent protein. Nat Biotechnol. 2004; 22:1567–1572. [PubMed: 15558047]
15. Choi CK, Vicente-Manzanares M, Zareno J, Whitmore LA, Mogilner A, Horwitz AR. Actin and alpha-actinin orchestrate the assembly and maturation of nascent adhesions in a myosin II motor-independent manner. Nat Cell Biol. 2008; 10:1039–1050. [PubMed: 19160484]

16. Vicente-Manzanares M, Koach MA, Whitmore L, Lamers ML, Horwitz AF. Segregation and activation of myosin IIB creates a rear in migrating cells. J Cell Biol. 2008; 183:543–554. [PubMed: 18955554]
17. Breckenridge MT, Dulyaninova NG, Egelhoff TT. Multiple regulatory steps control mammalian nonmuscle myosin II assembly in live cells. Mol Biol Cell. 2009; 20:338–347. [PubMed: 18971378]
18. Sprague BL, McNally JG. FRAP analysis of binding: proper and fitting. Trends Cell Biol. 2005; 15:84–91. [PubMed: 15695095]
19. Maupin P, Phillips CL, Adelstein RS, Pollard TD. Differential localization of myosin-II isozymes in human cultured cells and blood cells. J Cell Sci. 1994; 107(Pt 11):3077–3090. [PubMed: 7699007]
20. Nayal A, Webb DJ, Brown CM, Schaefer EM, Vicente-Manzanares M, Horwitz AR. Paxillin phosphorylation at Ser273 localizes a GIT1-PIX-PAK complex and regulates adhesion and protrusion dynamics. J Cell Biol. 2006; 173:587–589. [PubMed: 16717130]
21. Zaidel-Bar R, Milo R, Kam Z, Geiger B. A paxillin tyrosine phosphorylation switch regulates the assembly and form of cell-matrix adhesions. J Cell Sci. 2007; 120:137–148. [PubMed: 17164291]
22. Schneider IC, Hays CK, Waterman CM. Epidermal growth factor-induced contraction regulates paxillin phosphorylation to temporally separate traction generation from de-adhesion. Mol Biol Cell. 2009; 20:3155–3167. [PubMed: 19403690]
23. Worthylake RA, Lemoine S, Watson JM, Burridge K. RhoA is required for monocyte tail retraction during transendothelial migration. J Cell Biol. 2001; 154:147–160. [PubMed: 11448997]
24. Sandquist JC, Means AR. The C-terminal tail region of nonmuscle myosin II directs isoform-specific distribution in migrating cells. Mol Biol Cell. 2008; 19:5156–5167. [PubMed: 18843042]
25. Craig R, Woodhead JL. Structure and function of myosin filaments. Curr Opin Struct Biol. 2006; 16:204–212. [PubMed: 16563742]

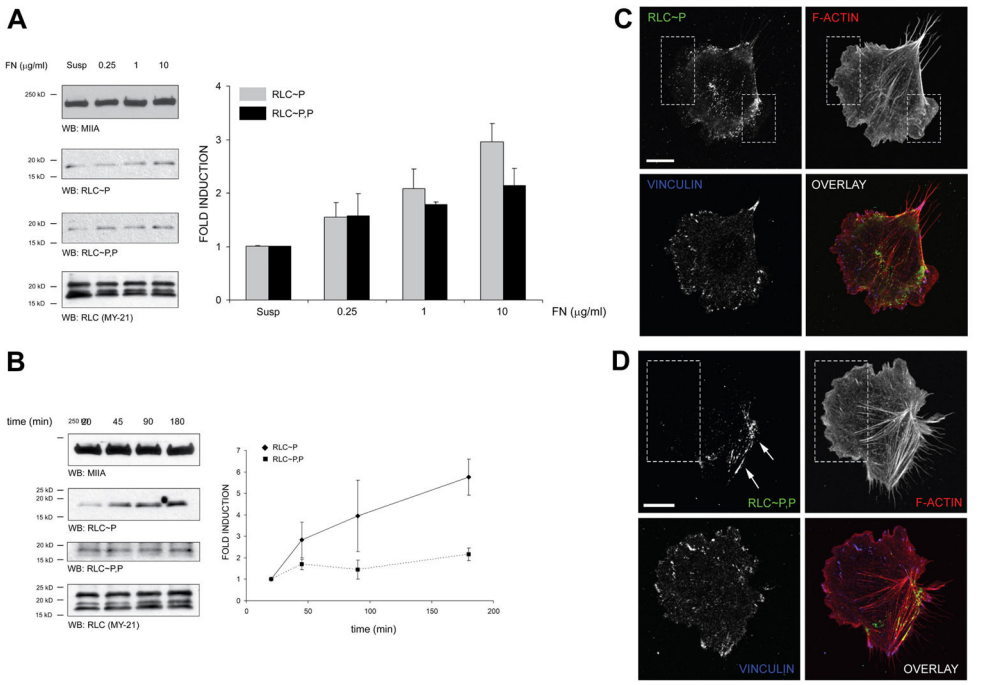

Figure 1. Adhesion to fibronectin promotes RLC mono (Ser19)- phosphorylation (RLC~P) and di (Thr18+Ser19)-phosphorylation (RLC~P,P) in an asymmetric manner

(A) CHO.K1 cells were plated for 45 min on different doses of fibronectin. Cells were then lysed, proteins separated by SDS/PAGE, transferred to PVDF membranes and probed for RLC~P and RLC~P,P by immunoblotting. Membranes were also probed for MHCII-A (top) and then reprobed for total RLC (bottom). A representative experiment out of three performed is shown. Right, densitometric analysis of the three experiments performed in these conditions. Average fold induction ± standard deviation is calculated with respect to the normalized value for suspended cells.

(B) CHO.K1 cells were plated for the indicated time points on 1 μg/ml fibronectin-coated dishes and probed as in (A). A representative experiment out of three performed is shown. Right, densitometric analysis as in (A). Data is normalized with respect to the value at 20 min.

(C–D) CHO.K1 cells were plated for 45 min on 2 μg/ml fibronectin-coated coverslips, fixed and permeabilized. RLC~P (C) and RLC~P,P (D) were then visualized by indirect immunofluorescence. Cells were co-stained as indicated to visualize F-actin (using phalloidin) and vinculin to visualize adhesions. Dotted boxes denote protrusions, which contain RLC~P, but not RLC~P,P; arrows point to RLC~P,P-decorated bundles. Representative cells from >200 visualized are shown. Bar = 10 μm.

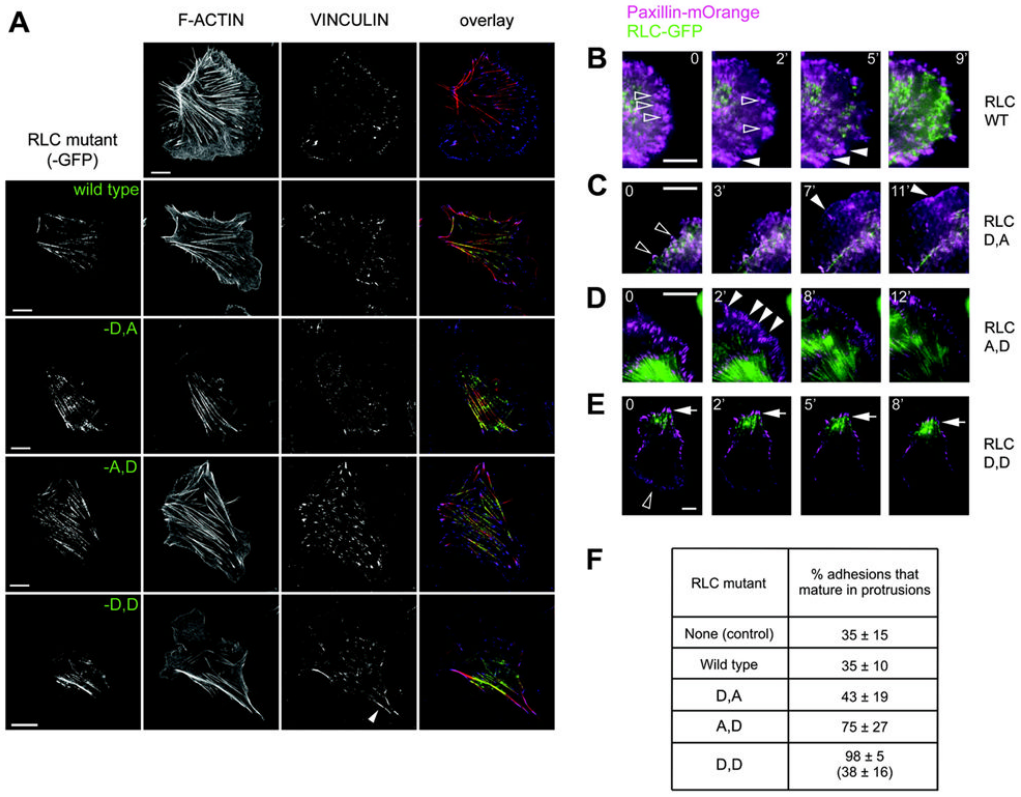

RLC mutant	% adhesions that mature in protrusions
None (control)	35 ± 15
Wild type	35 ± 10
D,A	43 ± 19
A,D	75 ± 27
D,D	98 ± 5 (38 ± 16)

Figure 2. Effect of mono and diphosphomimetic mutants on on adhesion maturation and polarity in migrating CHO.K1 cells

(A) CHO.K1 cells were transfected with the indicated mutant of RLC, RLC-18D,19A (RLC-D,A), -18A,19D (RLC-A, D), or 18D,19D (RLC-D,D), coupled to GFP (green), plated for 45 min on 2 μg/ml fibronectin-coated coverslips, fixed and stained for endogenous vinculin to visualize adhesions (blue) and with phalloidin to visualize F-actin (red). Representative cells from >200 visualized are shown. Bar = 10 μm

(B–E) Representative time-lapse images of protrusions in cells expressing comparable amounts of *wild type* RLC (B) or the D,A (C), A,D (D), or D,D (E) mutants coupled to GFP (green), and paxillin-mOrange (magenta). Hollow arrowheads point to representative adhesions that turn over, solid arrowheads point to adhesions that mature over the course of the experiment. Bar = 5 μm (except RLC-D, D, where bar = 10 μm).

(F) Percent of adhesions undergoing maturation in cells expressing the RLC mutants. Only cells expressing comparable amounts of the RLC mutant were analyzed. For RLC-D,D, the value on top corresponds to adhesions in the rear where RLC-D,D is concentrated; the value on the bottom corresponds to adhesions forming in protrusions opposite the rear. Data are the mean ± SD of ~30 cells (n≥150 in each case) from three independent experiments.

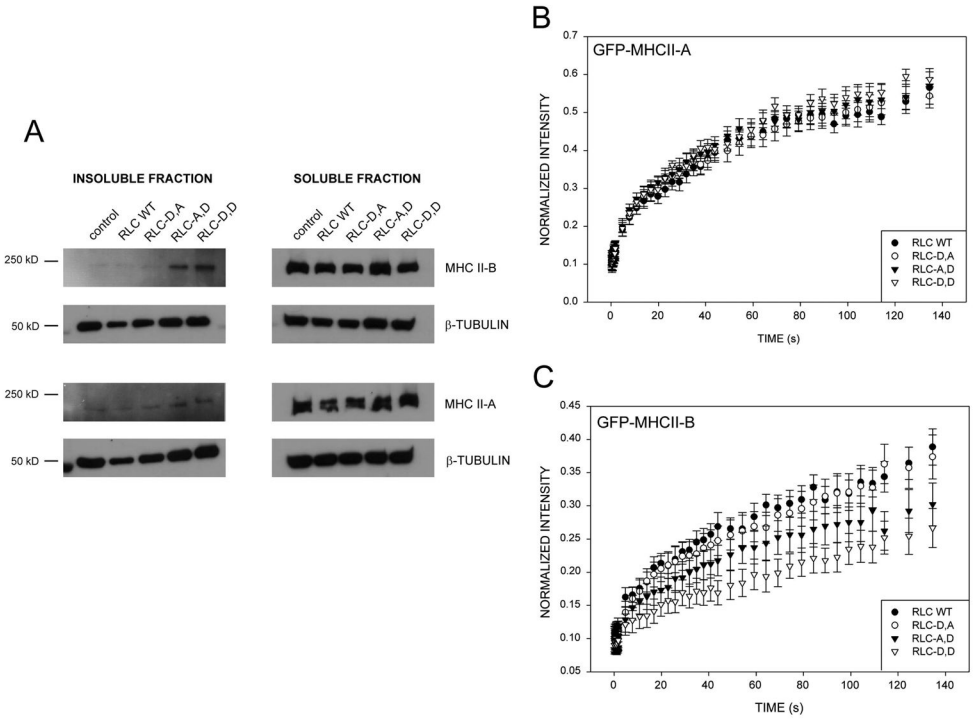

Figure 3. RLC mono- and di-phosphomimetic mutants induce differential assembly and stability of MHCII-B, but not MHCII-A

(A) CHO.K1 cells were transfected with the indicated RLC mutant, plated on 1 μg/ml fibronectin-coated dishes for 45 min, lysed (see M&M) and centrifuged; the supernatant is the soluble fraction (right). The pellet was solubilized with RIPA, constituting the insoluble fraction (left). Both fractions were blotted for endogenous MHCII-A and -B. β-tubulin is used as a loading control as its solubility is not affected by expression of the mutants. A representative experiment out of four is shown.

(B–C) CHO.K1 cells were co-transfected with GFP-coupled MHCII-A (B) and GFP-MHCII-B (C) and the indicated phosphomimetic mutants of RLC coupled to mCherry, plated for 45 min on 2 μg/ml fibronectin-coated coverslips.

Fluorescence recovery after photobleaching (FRAP) was then measured on actomyosin bundles, decorated with both fluorescent proteins (note that myosin IIA and IIB do not overlap in bundles). Data are the mean ± SE of 36 individual measurements per condition in four independent experiments.